Aeroacoustic Measurements from the Aerodynamic and Acoustic Rotorprop Test (AART) in the National Full-Scale Aerodynamics Complex (NFAC) 40- by 80-Foot Wind Tunnel

James H. Stephenson
U.S. Army Combat Capabilities Development Command Aviation & Missile Center Hampton, VA, USA

Natasha L. Schatzman
NASA Ames Research Center Moffett Field, CA, USA

Benny K. Cheung
NASA Ames Research Center Moffett Field, CA, USA

Nikolas S. Zawodny
NASA Langley Research Center Hampton, VA, USA

D. Caleb Sargent
Sikorsky Aircraft, a LMCO Stratford, CT, USA

Ben Wel-C. Sim [*]
U.S. Army Combat Capabilities Development Command Aviation & Missile Center Moffett Field, CA, USA

ABSTRACT

Unmanned Aerial Vehicle (UAV) designs typically have aerodynamic configurations that result in complex aerodynamic and acoustic conditions, such as wing and propeller interaction. In response, the Aerodynamic and Acoustic Rotorprop Test (AART) Program was implemented, a primary objective of which was to determine the aerodynamics and acoustics related to an auxiliary propulsor mounted behind an isolated wing in the National Full-Scale Aerodynamics Complex (NFAC) 40-by 80-Foot Wind Tunnel. Three configurations (no wing, half wing, and full wing) were tested, with conditions including variation of the propeller speed, wind tunnel Mach number, and yaw. The acoustic setup, processing, and analysis are discussed along with the known issues for this complex data set. The interaction of upstream bodies and the resulting substantial increase in acoustic emissions are detailed.

NOTATION

AART   Aerodynamic and Acoustic Rotorprop Test

Azi.   Azimuth angle of microphone, counter clockwise as seen from above starting from the downstream direction.

BG   Background

BPF   Blade pass frequency (Hz)

C_T Propeller thrust coefficient, $T/\rho\omega^2 D^4$

C_P Propeller power coefficient, $P/\rho\omega^3 D^5$

Dist.   Total distance from propeller hub to microphone

D   Propeller diameter

Elv.   Elevation angle of microphone, $0°$ denotes horizon plane, $-90°$ is directly below the propeller

M_{TUN} Wind tunnel freestream Mach number

NFAC   National Full-Scale Aerodynamics Complex

L   Overall sound pressure level (dB)

P   Propeller Power

P_{ref} Sound pressure level reference pressure (20 μPa)

R   Propeller radius

RPM   Propeller rotational speed, revolutions per minute

SPL   Sound pressure level (dB)

T   Propeller thrust

V_∞ Tunnel freestream velocity

X   Upstream coordinate relative to propeller hub, negative into the wind

Y   Lateral coordinate relative to propeller hub, positive starboard

Yaw   Rotation measured normal to tunnel flow (deg)

Z   Vertical coordinate relative to propeller hub, positive up

ω Propeller rotational speed (revolutions/sec)

Ω Propeller rotational speed (revolutions/minute)

ρ Density of air

INTRODUCTION

The Unmanned Aerial Vehicle (UAV) and Urban Air Mobility (UAM) markets are growing and contain multiple vehicle designs where propellers and/or rotors are ingesting aerodynamic turbulence from upstream bodies (Ref. 1). Further, Sikorsky, A Lockheed Martin Company, and the U.S. Army have been developing multiple platforms in support of Future Vertical Lift that employ pusher propeller technology. There is a strong need to understand the complex aerodynamic and aeroacoustic emissions of these vehicles, to assess current and future technologies, and to limit community noise exposure (Refs. 2–4).

A significant body of research has been devoted to investigating the effects of pusher propeller configurations on vehicle acoustic emissions (Refs. 5–9). It is known that the wake deficit from upstream bodies causes nonuniform inflow as well as increased turbulence ingestion into the propeller system (Ref. 5). It is the modification of the inflow to the propeller system, which results in unsteady aerodynamic loads and increased acoustic emissions for pusher propellers. The increased acoustic emissions are known to be prominent outside of the propeller tip path plane (Ref. 7). Loading noise is known to be at a minimum in the tip path plane, and this explains why the acoustic impacts of pusher propeller configurations are most noticeable outside of the propeller plane. This has also been seen in other unsteady aerodynamic loading environments, such as those experienced by a rotor in a recirculating flow (Refs. 10, 11).

Previous experiments on pusher propeller acoustic emissions have suffered due to limitations in either their acoustic measurement capability or in their aerodynamic measurement capability. Thus, the U.S. Army and Sikorsky have introduced the Aerodynamic and Acoustic Rotorprop Test (AART) program to meet this need. The AART program objective, which expands on the prior work of Ref. 12, is to acquire the aerodynamic and aeroacoustic response of a canonical wing and propeller interaction.

In 2018, the AART test stand, which is comprised of an auxiliary propulsor mounted behind an isolated wing in various configurations, was tested in the Army 7- by 10-Foot Wind Tunnel at the NASA Ames Research Center. The 2018 comprehensive aerodynamics test consisted of force measurements from the propeller system and in-flow stereo particle image velocimetry (PIV) measurements.

With the support of NASA, the AART stand was subsequently tested in the National Full-Scale Aerodynamics Complex (NFAC) 40- by 80-Foot Wind Tunnel from 2019–2020. That experiment, described here, was conducted to determine the associated acoustics emissions for the previously tested aerodynamic conditions with the intent of providing high quality acoustic and complementary aerodynamic data for modeling efforts.

EXPERIMENTAL SETUP

The experimental setup is now described, including the test hardware, data instrumentation and acquisition, and the relevant test conditions.

Test Hardware

The AART stand was mounted in the NFAC on a three-strut support structure that rotates on the test-section turntable. Figure 1 shows the downstream view of the AART stand with the full wing configuration in the NFAC 40- by 80-Foot Wind Tunnel. The walls and floor of the test section are treated with acoustically absorbent material to reduce acoustic reflections, providing an absorptivity of greater than 90% at frequencies above 100 Hz (Ref. 13).
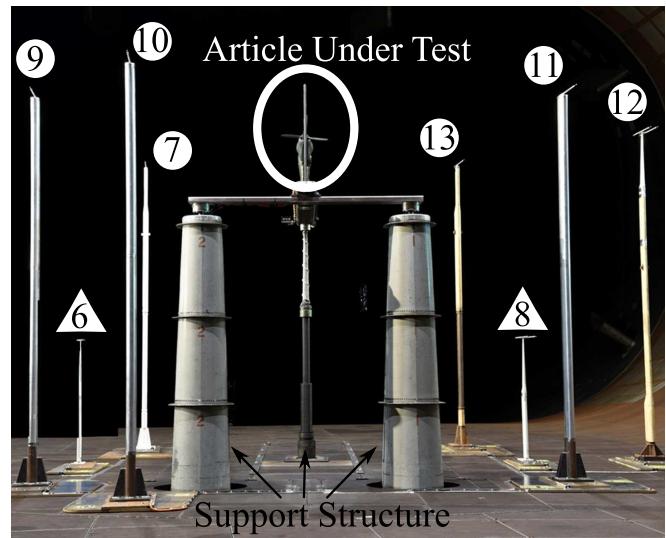
Figure 1. AART with microphone locations in the NFAC 40- by 80-Foot Wind Tunnel test section, view looking downstream.

The AART stand consists of a Sensenich L26H off-the-shelf 26 inch diameter propeller with the option of three upstream wing configurations: no wing, half wing (40.5 inch), and full wing (58.5 inch), seen in Fig. 2. The half wing condition extends from below the propeller, through the hub height, and ends 4.365 inches below the propeller tip. The full wing condition extends from below the propeller to above the propeller tip. The wing used is a NACA 0015 airfoil, 12 inch chord, at $0°$ angle of attack. It is located 4.45 inches upstream of the propeller plane, 3.5 inches in front of the hub, in all wing configuration cases.
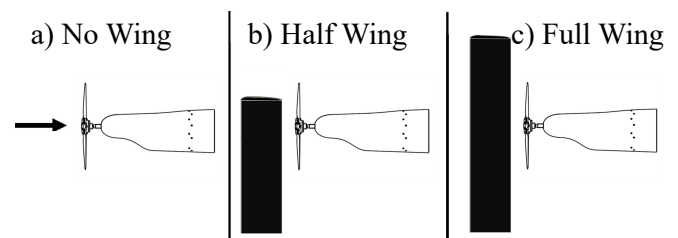
Figure 2. AART a) no wing, b) half wing, and c) full wing configuration.

Propeller thrust and torque measurements were acquired using an Able Task 2.0 MK XXXII balance, while eight microphones were placed around the AART stand to take acoustic measurements (Fig. 1). Microphones are free-field GRAS 40 AC $\frac{1}{2}$" with a GRAS 26 AJ $\frac{1}{2}$" preamplifier. Additionally, three beamform acoustic arrays (Ref. 14) were installed downstream, midstream, and upstream of the propeller plane. Acoustic measurement results from the beamform array systems are not presented in this paper.

All microphone locations are in the acoustic far-field (at least 10 radii from the hub). Microphones 6 and 8 were placed on 5.625 foot struts and microphones 7 and 9 through 13 were

placed on 15 foot struts on top of the acoustic liner on the turntable. Table 1 provides the X, Y, Z, distance, azimuth, and elevation of each microphone with respect to the propeller center. Here, the X-direction is positive toward the downstream direction, the Y-direction is positive starboard, toward the test section door, and the Z-direction is negative down. See Fig. 3 for a top view of microphone locations in the NFAC 40-by 80-Foot Wind Tunnel.

Table 1. Microphone positions with respect to center of the propeller.

Mic #	X [ft]	Y [ft]	Z [ft]	Dist. [ft]	Azi. [deg.]	Elv. [deg.]
6	-0.53	10.05	-9.18	13.6	93	-42
7	8.48	8.37	0.17	11.9	45	1
8	-0.56	-10.01	-9.19	13.6	267	-47
9	-10.03	10.37	0.12	13.4	134	0
10	-15.92	5.91	0.15	17.0	160	1
11	-9.98	-10.30	0.14	14.3	226	1
12	-0.38	-15.57	0.32	15.6	269	1
13	8.46	-8.35	0.12	11.9	315	1

Center of the coordinate system at the propeller hub

X: Upstream coordinate, negative into the wind

Y: Lateral coordinate, positive toward starboard

Z: Vertical coordinate, negative down

*Dist.: Total distance from propeller hub to microphone*

Azi.: Azimuth angle of microphone, counter clockwise as seen from above starting from the downstream direction.

Elv.: Elevation angle of microphone, $0°$ denotes horizon plane, $-90°$ is directly below the propeller.

Microphones 7 and 9 through 13, are at an elevation angle of approximately 0 degrees and have an azimuthal spacing approximately every 45 degrees. This provides a close to uniform azimuthal distribution to validate modeling and simulation tools. Microphones 6 and 8 are inline with the propeller plane in order to assess symmetry and acquire data in the direction that most affects the community during flyover conditions.

Data Instrumentation and Acquisition

The acoustic data recording setup is shown in Fig. 4 and consists of: NFAC Dynamic Data Acquisition system (DDAS), NASA supplied Dewetron DAQ, AART stand encoder, encoder conditioning box, 8 free-field microphones, and a microphone power supply. Each microphone was calibrated in situ using a GRAS Type 42AA pistonphone calibrator. Acoustic data were acquired at 250 kHz, while some of the aerodynamic data were acquired at a lower sampling rate. Raw acoustic data were converted from volts to acoustic pressure by using the individual microphone calibration constant and microphone gain setting. The acoustic pressure time history was then harmonically averaged. The 1/rev signal was used to identify the beginning of each revolution. Each revolution was
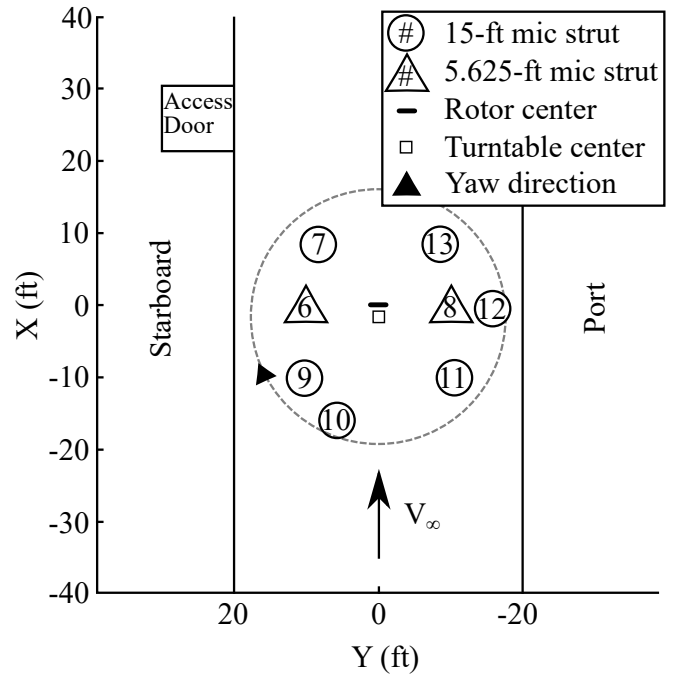
Figure 3. AART with microphone locations in the NFAC 40- by 80-Foot Wind Tunnel test section, top view.

then interpolated to a constant sample size. The revolutions were averaged to create a single time history representative of approximately 1,250 revolutions. Acoustic spectra were then calculated using 15 repetitions of the ensemble-averaged pressure time histories.

Repeating the ensemble-averaged time history to calculate spectral characteristics suppresses uncorrelated broadband noise from the tunnel and propeller system alike, effectively increasing the signal-to-noise ratio. Harmonic values above the facility background noise are unaffected by this process, and an approximation of the harmonic values below the background noise becomes possible.

Test Conditions

AART Test Conditions: The AART stand and wind tunnel were operated in a wide range of test conditions. The core test conditions are documented here, along with some auxiliary data collection for quality assurance. The stand was tested for all three wing configurations, with blades on and off, at tunnel freestream Mach numbers ranging from 0.110 to 0.222. The propeller pitch was held constant at $24°$, and propeller speed varied between 3000 and 7100 RPM. The test stand was oriented predominantly at $0°$ yaw, with an additional data set at $5°$ yaw. Microphones 6 through 13 are on the wind tunnel turn table, and so their orientations as reported in Table 1 remain constant. During yawed test conditions, each microphone strut was rotated to maintain a minimal angle direction into the wind to minimize aerodynamic influence.

Pistol Reflection Test: Prior to the start of the blade-on testing, a Pistol Refection Test (PRT) took place with the doors

3
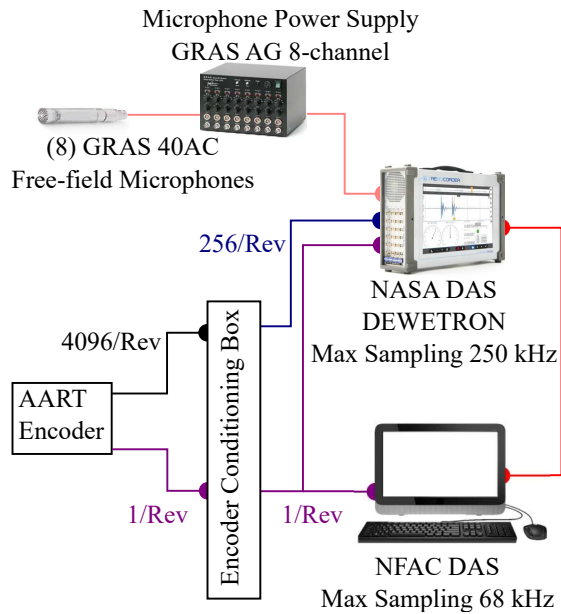
Figure 4. NFAC 40- by 80-Foot Wind Tunnel acoustic data collection setup.

Figure 5. Pistol Reflection Test shooter pointing into the wind at the propeller hub center of the AART propeller.

closed, wind off, and no wing. A Winchester Symbol X22SB starter pistol was used with Winchester 0.22 Caliber Short Blanks. The pistol produced a distinct impulsive signature and is used to identify reflections due to the presence of the microphone struts and auxiliary test hardware. The starter pistol operator was placed on a scissor lift at approximately 15 feet in the air as close to the AART hub as possible, with hearing protection on, and wind tunnel door closed. The starter pistol was fired straight upstream from where the center of the AART propeller would be located (see Fig. 5). No pistol reflection tests were conducted with the half or full wing in place, so potential reflections from the wing are not captured.

Background Noise Conditions: Wind tunnel background noise is a combination of wind noise over the microphones, test hardware, AART stand mechanical noise, and the wind tunnel drive noise. To measure the background noise for this test setup, the wind tunnel was operated at all core test conditions without the propeller blades present, but with the hub spinning and all other test hardware present.

DATA QUALITY ANALYSIS

Before analysis of the acoustic trends from the AART propeller are presented, a data quality assessment is performed. This assessment includes the pistol reflection test, background noise analysis, signal-to-noise, and repeatability in terms of revolution-to-revolution and point-to-point comparisons. It is important to note that a 'point' in the NFAC refers to measurements taken at a specified condition, and so point-to-point comparison is a measure of the repeatability for the same nominal wind tunnel and test stand configuration. A subset of the data quality analysis is provided here.
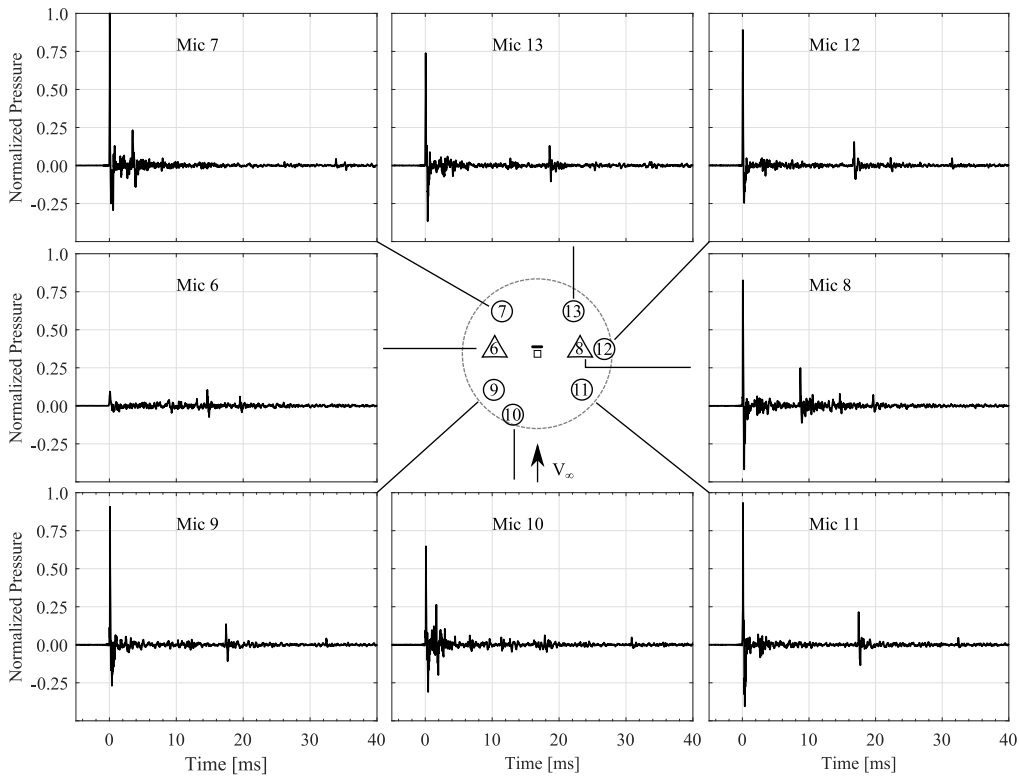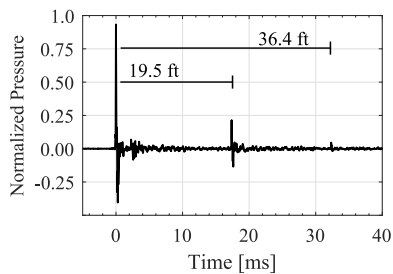
Pistol Reflection Test

During each of the PRT shots, acoustic data were recorded for all microphones starting prior to the firing of the starter pistol and extending for 15 seconds after, to ensure any reflections were recorded. A pressure time history result from one of the PRT shots is shown in Fig. 6 for all microphones, where the pressures have been normalized by the peak pressure of approximately 80 Pa, and the time index has been adjusted to the arrival time of the incident pulse. Each subfigure is labeled with its associated microphone, and an additional line is used to show where each microphone is located relative to the wind and article location, as seen in Fig. 3. This PRT shot reveals reflections for all microphones that could be due to microphone struts, test stand, or the scissor lift. Microphone 6 shows an anomalously small incident wave that is a result of shielding from the steel scissor lift platform, which is in direct line of sight between the propeller hub and this microphone during the PRT test.

A closer look at the PRT results are shown in Fig. 7 for microphone 11. Figure 7 shows the acoustic time history in milliseconds, where three distinct pulses are identifiable. The first pulse is the direct pulse from the shot, while the second and third pulses are reflections from surrounding surfaces. The first and second pulses have a distinct sharp initial rise. Pulse 3 is significantly attenuated, and it is harder to distinguish the sharp initial rise. The time delay between pulse 1 and 2 suggests a travel difference of approximately 19.5 feet, and approximately 36.4 feet from pulse 1 to 3.

It is highly likely that pulse 2 is a reflection off the turntable floor, as the time delay between the pulses is equivalent to the geometric difference for a ground reflection. This is true for all of the primary acoustic reflections measured by the microphones, and is likely caused by the steel plate used to mount

Figure 6. Pistol reflection test results for all microphones.

Figure 7. Pistol reflection test for microphone 11.

each microphone stand to the ground. It should be noted that the amplitude of the primary reflection is substantial in each of the microphone measurements and should be considered when examining the acoustic data. An investigation is ongoing to attempt to remove the reflections from the measured data.

Background Noise

A comparison of the background noise for the no wing, half wing, and full wing conditions at M_{TUN} = 0.204, Yaw = 0°, Pitch = 0°, and Ω = 6300 is shown in Fig. 8. Each subfigure in Fig. 8 shows the spectra calculated in half second blocks with 50% overlap, for a 30 second time interval. The microphone number is appended to each subfigure, and the Overall Sound Pressure Level (OASPL, L) for each wing configuration condition is shown in the legend. For this paper, the OASPL is the integrated level between 100 Hz and 5 kHz and contains all of the primary frequencies of interest. Thus, the first (top

left) subfigure shows microphone 7 recorded OASPL values of 102.1, 102.2, and 102.1 dB for the no wing, half wing, and full wing configurations, respectively.

Minimal OASPL differences are shown for each microphone among all configurations. In general, with a few outliers, the OASPL increases as the half wing and full wing are added, which is due to the aerodynamic disturbances of the added components. Furthermore, the 5.625 ft strut microphones (6 and 8) reveal a higher OASPL compared to the 15 ft struts; this is due to differences in strut design and strut location.

The effect of yaw (0° and 5°) on background noise for the full wing configuration was also investigated. For a similar operating condition as before, an analysis of the background noise data yielded an OASPL difference as low as 0.2 dB between yaw conditions. On average, all microphones were within 3 dB and no clear qualitative observation could be determined to state that increasing yaw has an overall increase or decrease in OASPL for background noise for this test.

Signal-to-Noise Analysis

The signal-to-noise ratio was of particular concern for this test as the propeller was expected to be relatively quiet compared to the background noise of the facility. To improve signal acquisition, the microphone struts were placed close to the propeller while still being in its acoustic far-field. An analysis of the signal-to-noise is presented here comparing the background noise (blades off) to blades on for the first ten blade pass frequencies (BPF).
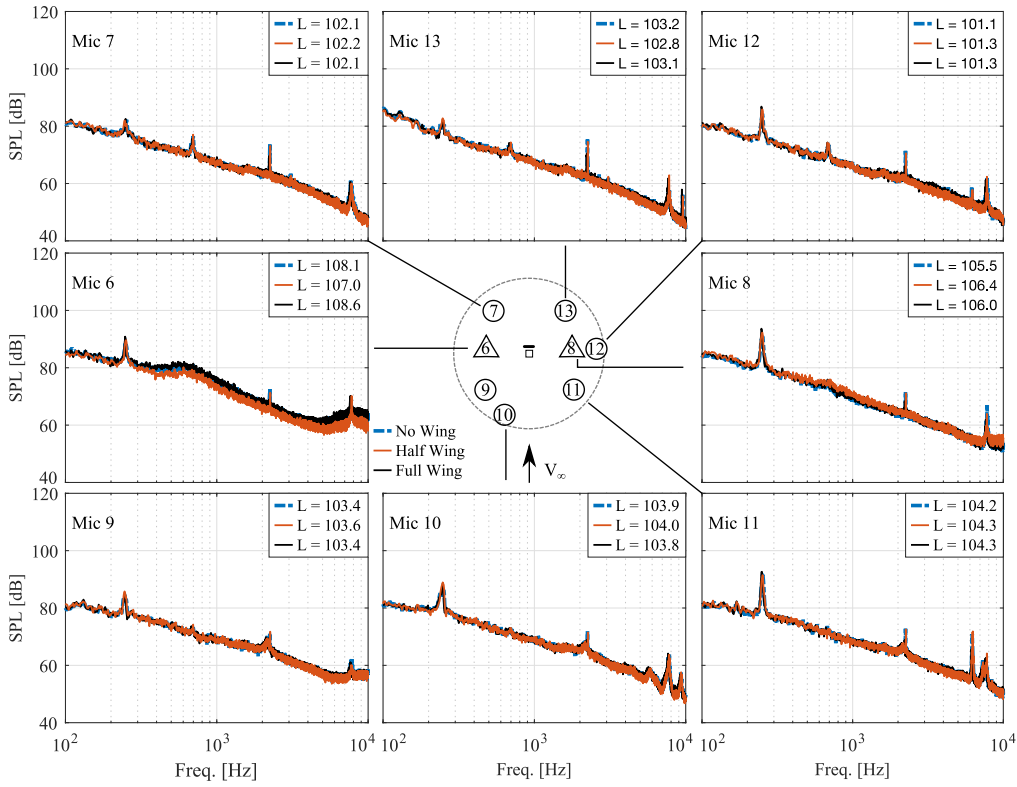
Figure 8. Background noise for no wing (dashed blue), half wing (solid orange), and full wing (solid black) (M_{TUN} = 0.204, Yaw = 0°, Ω = 6300). OASPL (L) provided on each subplot in units of dB (ref. 20 μPa).

The configuration with no wing is the most concerning due to the low signal of the propeller. Figures 9 and 10 show the time history and frequency spectra, respectively, for background noise (blades off) versus blades on, for an operating condition with no wing and M_{TUN} = 0.204, Yaw = 0°, and Ω = 6300.

Figure 9 shows the ensemble-averaged pressure time history for the no wing condition, with the lines indicating the averaged value and the corresponding shaded region indicating standard deviation at each time stamp. Standard deviations are broken up into 25% of each plot, so that they do not overlap each other and remain visually intelligible.

Some obvious trends can be seen in the figure and are expected, such as the low acoustic emission forward of the propeller (microphone 10), and more prominent emissions off to each side (microphones 6, 8, and 12). Microphone 6 shows an uncharacteristic double-hump shape, which is very likely caused by a strong reflection. Microphones 8 and 12 also show some unexpected differences; they should be near identical measurements as the only difference is an elevation angle change, which has negligible effect for an isolated propeller at zero angle of attack.

Most concerning in Fig. 9 is the standard deviation shown by the shaded region. The forward microphones (9-11) show the least revolution to revolution changes, with a resulting standard deviation approximately four times greater (4 Pa) than the peak pressure amplitudes (1 Pa). The background noise measurements have similar standard deviations for these microphones, showing that the data are dominated by the wind

and facility noise on the microphones. Microphones 7 and 13 show the largest standard deviation with the standard deviations extending well beyond the range of the plot (greater than 8 Pa). This is a lesson learned for the authors, as these microphones are in the wake of upstream microphones and so suffer from additional noise.

The no wing configuration produces the lowest acoustic emissions at this speed; the steady loading noise for this condition is quite low, as evidenced by the very small C_T values (C_T = 0.055), and there is no additional unsteady loading caused by upstream disturbances. Further, at this high tunnel Mach number (M_{TUN} = 0.204), the wind and facility noise is at its peak. This condition has the unfortunate combination of low signal and high noise, making it one of the worst signal-to-noise conditions in the test.

Spectral representation for the no wing configuration is shown in Fig. 10. Here, the revolution averaged background noise is shown in the solid line, while the gray dotted line shows the half-second averaged spectra. The blue dashed line has solid circles at each of the first ten harmonics to help facilitate interpretation of the harmonic noise. The first BPF sound pressure level is generally above the half-second averaged facility noise for this condition in all directions, and many of the lower harmonics are above the revolution averaged background noise. In general, however, the harmonic amplitudes above the second BPF are not trustworthy, due to low signal-to-noise ratio for this condition.

The half wing and full wing conditions show significantly bet-
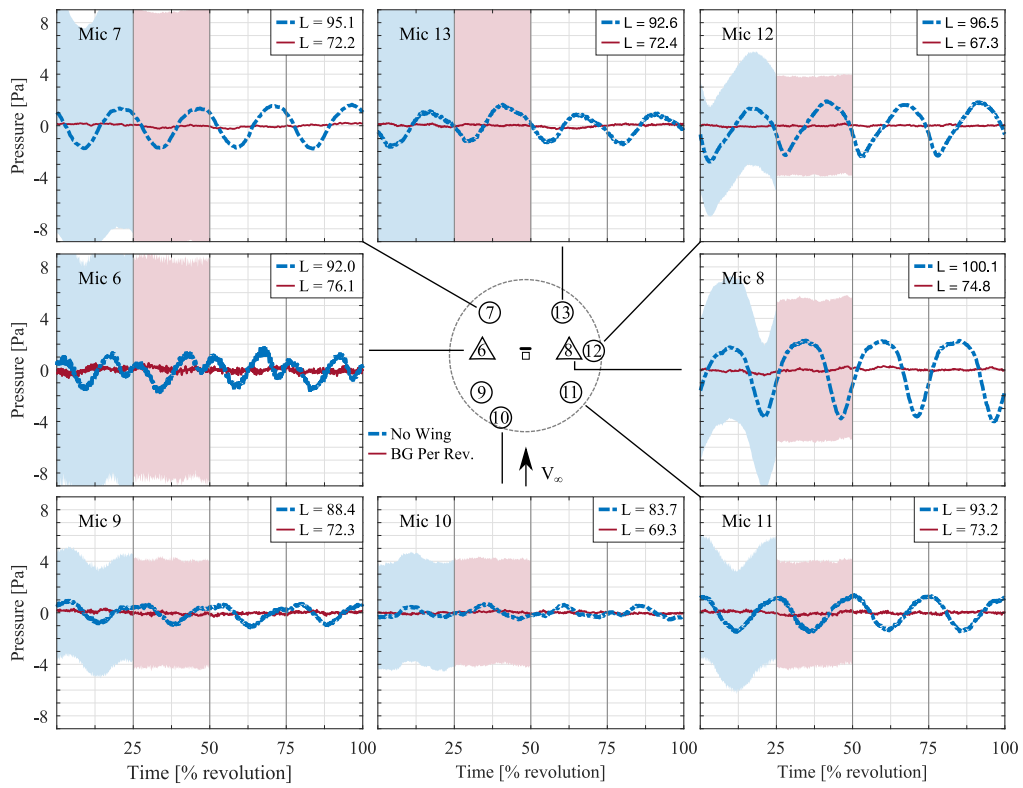
Figure 9. Signal-to-Noise acoustic time history comparison between blades off and on for no wing configuration for a condition of M_{TUN} = 0.204, Yaw = 0°, Ω = 6300, C_T = 0.055, and C_P = 0.080. Blades off condition is identified as the background (BG) noise for this and future conditions. OASPL (L) provided on each subplot in units of dB (ref. 20 μPa).
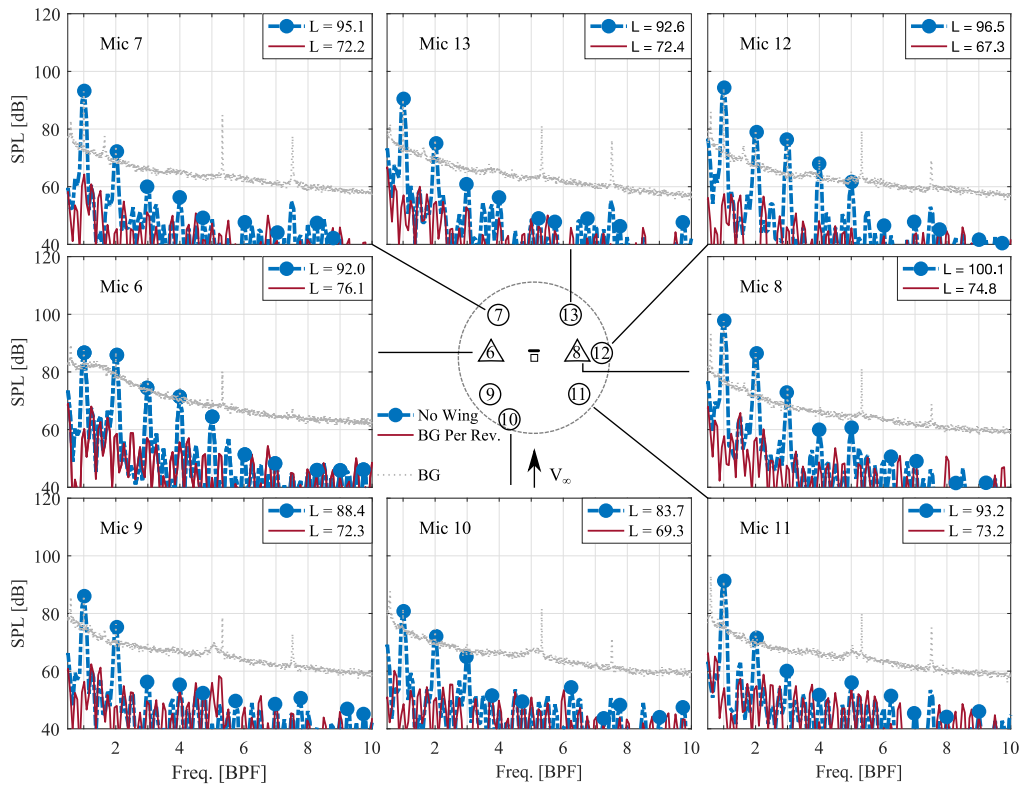
Figure 10. Signal-to-Noise frequency spectra comparison between blades off and on for no wing configuration for condition identical to Fig. 9. OASPL (L) provided on each subplot in units of dB (ref. 20 μPa).

ter signal-to-noise for the high tunnel Mach number points. Figure 11 shows the ensemble-averaged pressure time history for the full wing configuration, for the same condition as before ($M_{TUN} = 0.204$, Yaw = 0°, $\Omega = 6300$).

Here the standard deviation remains at approximately 4 Pa in the forward microphones, but the peak pressures for this condition are also approximately 4 Pa. The rear microphones still have significant standard deviations due to ingesting the upstream flow, and the sideline microphones (6, 8, 12) show the same irregularities as previously mentioned.

The resulting spectra for this full wing condition is shown in Fig. 12. Observe that the majority of the harmonics are well above the background noise of the facility, giving significantly more confidence in the wing conditions than the no wing condition for the high tunnel Mach number cases. However, the high standard deviation caused by revolution to revolution differences remains a concern.

Point-to-Point Repeatability

The repeatability of the acoustic data has been analyzed in terms of revolution-to-revolution variation by the discussion of the standard deviation above; however, a critical measure of repeatability is captured by a point-to-point variation analysis. The point-to-point comparison is performed by comparing the results of multiple wind tunnel data acquisition points for the same nominal test condition. It should be noted that a wind tunnel 'run' is defined as a single operation of the wind tunnel (from start up to shut down), while a 'point' is a unique test condition within a given run. Thus, there are typically many points acquired in a single run.

Figure 13 shows a point-to-point comparison for no wing configuration for an operating condition of $M_{TUN} = 0.204$, Yaw = 0°, and $\Omega = 6230$, in which each point is from the same wind tunnel run. A minimal difference is shown between each point, with a maximum OASPL difference less than 1.5 dB for these points and significant repeatability shown in the ensemble-averaged time histories. Microphone 6 shows that the reflections impacting the data are a constant between runs, lending some hope that future research will be able to remove the reflection noise from the results. The standard deviations between each run are also shown to be fairly constant. Overall, the test stand and wind tunnel are shown to produce reliable results for nominally identical test conditions.

RESULTS

The data quality analysis has shown remarkable repeatability between points. The analysis also showed quality signal-to-noise ratios for the wing configurations, and unfortunately some significant reflections from the facility and test stand. With confidence in the data quality now understood, and the reflection limitation in mind, an analysis of the primary data can be conducted.

Comparisons between wing configuration, RPM, wind tunnel Mach number, and yaw are presented. Though a wide varia-

tion of these parameters is available, only a select few cases are provided for the sake of brevity.

Wing Configuration Comparison

In helicopter and propeller acoustics, the pressure time history typically reveals the physical mechanisms that result in the acoustic tonal emissions, more so than the spectral content. This is because the acoustic emissions at the harmonics are amplified due to the rotational nature of the system, and so most mechanisms fall on harmonics of the blade passage frequency, making it difficult to separate the components in frequency space. As such, the pressure time histories will be the predominant figures investigated.

Figure 14 shows a pressure time history comparison between wing configurations for an operating condition of $M_{TUN} = 0.111$, Yaw = 0°, and $\Omega = 6500$. The no wing condition shows the expected results. Pressure amplitudes peak in the propeller plane of rotation (microphones 6, 8, and 12), predominantly driven by the thickness noise. Pressure amplitudes decrease in the fore and aft directions as the loading noise is small for this propeller in comparison to the thickness noise components. This is the first look at a lower tunnel Mach number ($M_{TUN} = 0.111$), and it should be noted that the standard deviations for these conditions are significantly better than those seen previously due to reductions in wind and facility noise. The downstream microphones (7 and 13) still significantly suffer from wake ingestion from the upstream microphones, and microphone 6 is still dominated by the reflections, but the remaining microphones show high quality results.

The half wing and full wing configurations show a completely different pattern than what is seen for the no wing configuration. As expected, the upstream wing imparts an unsteady loading component on the propeller, which results in increased noise in the fore and aft directions. The assumption that this is caused by unsteady loading on the propeller is bolstered by the fact that the in-propeller plane (microphones 6, 8, and 12) acoustic emissions are less impacted by the presence of the wing than the out-of-plane microphones.

An impulsive negative to positive pressure peak with a peak-to-peak pressure of approximately 9 Pa is seen in the fore direction of the half wing configuration (Fig. 14, microphone 9). Similarly, microphone 11 shows a positive to negative pressure peak, with a peak-to-peak pressure of approximately 9 Pa. The full wing configuration shows a negative to positive impulsive pressure emission, with a peak-to-peak pressure of only 6 Pa. The change between negative to positive pressure amplitude for the half wing condition on microphone 9, to the positive to negative pressure amplitude on microphone 11 is attributed to the direction of rotation and asymmetric vertical load caused by the half wing on the propeller inflow.

The single largest takeaway from Fig. 14 is that each of the wing configurations produces a unique acoustic emission in all directions. This drives home the importance of understanding and accurately modeling the upstream bodies on pusher-propeller vehicles if acoustic emissions are to be predicted.
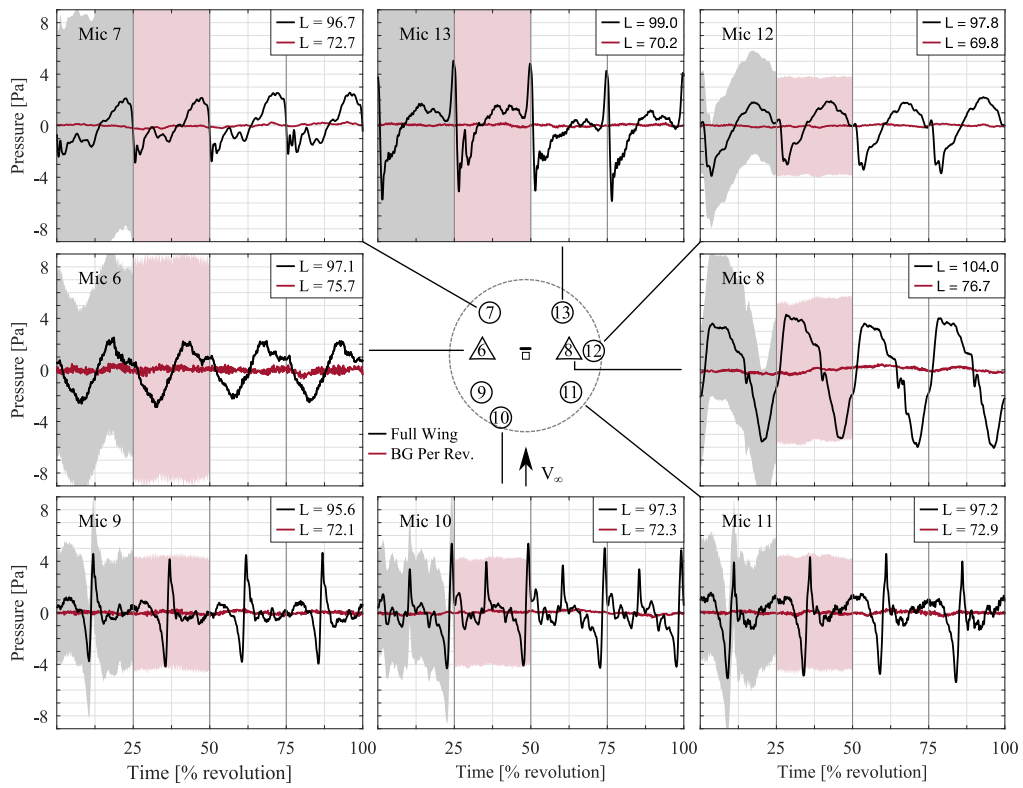
Figure 11. Signal-to-Noise acoustic time history comparison between blades off and on for full wing configuration for a condition of M_{TUN} = 0.204, Yaw = 0°, Ω = 6300, C_T = 0.062, and C_P = 0.084. OASPL (L) provided on each subplot in units of dB (ref. 20 μPa).
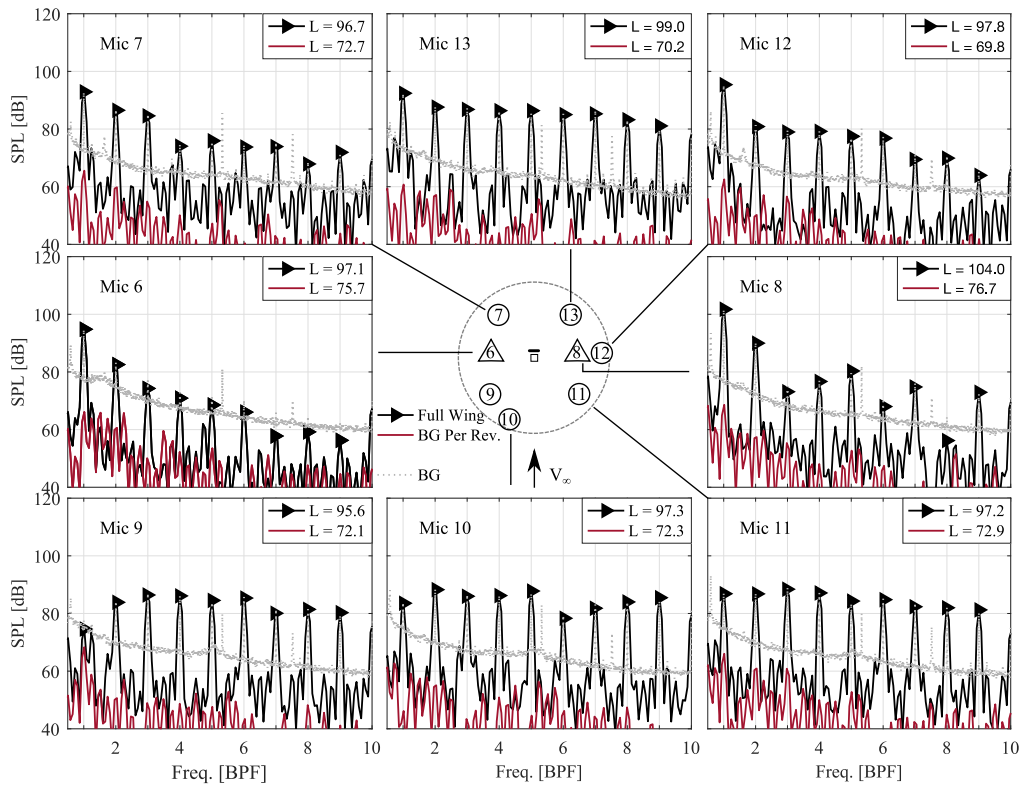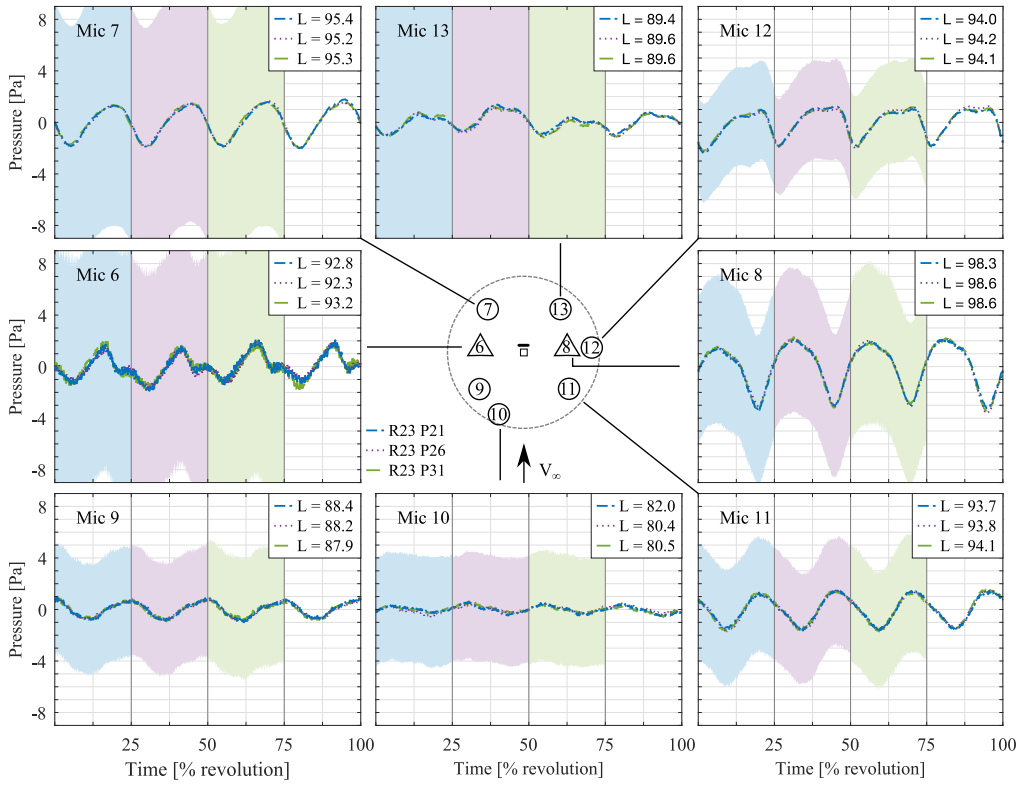

Figure 12. Signal-to-Noise frequency spectra comparison between blades off and on for full wing configuration for condition identical to Fig. 11. OASPL (L) provided on each subplot in units of dB (ref. 20 μPa).

9

Figure 13. Point-to-point acoustic time history comparison for no wing configuration for an operating condition of M_{TUN} = 0.204, Yaw = 0°, Ω = 6230, C_T = 0.051 ± 0.001, and C_P = 0.077 ± 0.000. OASPL (L) provided on each subplot in units of dB (ref. 20 μPa).

RPM Sweeps

During the test, multiple RPM sweeps were performed. Two of these RPM sweeps are presented and analyzed. An RPM sweep for the no wing configuration and an operating condition of M_{TUN} = 0.111, Yaw = 0°, and Ω swept from 6000 to 6500 RPM is now presented in Fig. 15. The no wing RPM sweep shown in this figure exhibits a complex acoustic emission pattern. Microphones 8 and 12 show the expected pattern for a propeller plane measurement location, where the sound pressure level increases with increasing tip speed (Ω R). In the forward direction, there is a general increase in noise with increasing Ω, however, it becomes somewhat more complicated due to the interplay of loading noise and thickness noise for the out-of-plane directions. Due to data quality concerns regarding the increased standard deviations in Microphones 7 and 13, and the strong reflections in Microphone 6, the authors refrain from examining that data too closely.

An RPM sweep for the full wing configuration is also investigated here, and is shown in Fig. 16 for similar conditions as seen in Fig. 15. As seen before, Microphones 8 and 12 show the expected increase in noise with increasing tip speed in the plane of the propeller. In the out-of-plane directions, the interplay between steady loading noise and thickness noise is further complicated by the addition of the unsteady loading noise created by the wing wake. The amplitude and pulse shape of the forward radiated noise change with increasing tip Mach

number, and may be a demonstration of the mutual influence of the propeller on the wing. This phenomenon should be investigated further and computationally modeled to elucidate the true physical mechanisms that resulted in these acoustic changes. However, as seen before in Fig. 14, the effect of the wing upstream of the propeller has produced near universal increases in the noise levels as compared to similar conditions for the no wing condition (Fig. 15).

Wind Tunnel Mach Number Sweep

A wind tunnel velocity sweep was performed for an operating condition of M_{TUN} = 0.111-0.204, Yaw = 0°, and Ω = 6200 for the no wing configuration. Figure 17 shows the pressure time histories for all microphones for this condition. For this condition, the noise from the propeller system in the no wing configuration generally decreases with increasing tunnel Mach number. This is primarily due to the decreasing steady loading noise, as the thrust coefficient (C_T) drops from 0.178 at the lowest tunnel speed, to 0.052 at the highest tunnel speed. Another major take away is the increase in the standard deviation at each microphone location, from the lowest speed to the higher tunnel speeds. This is due to the increase in the wind and facility noise at higher tunnel Mach numbers. The increase in the standard deviation at the higher tunnel speeds is one major reason why the figures in the Results section focus on the low Mach number cases.

10
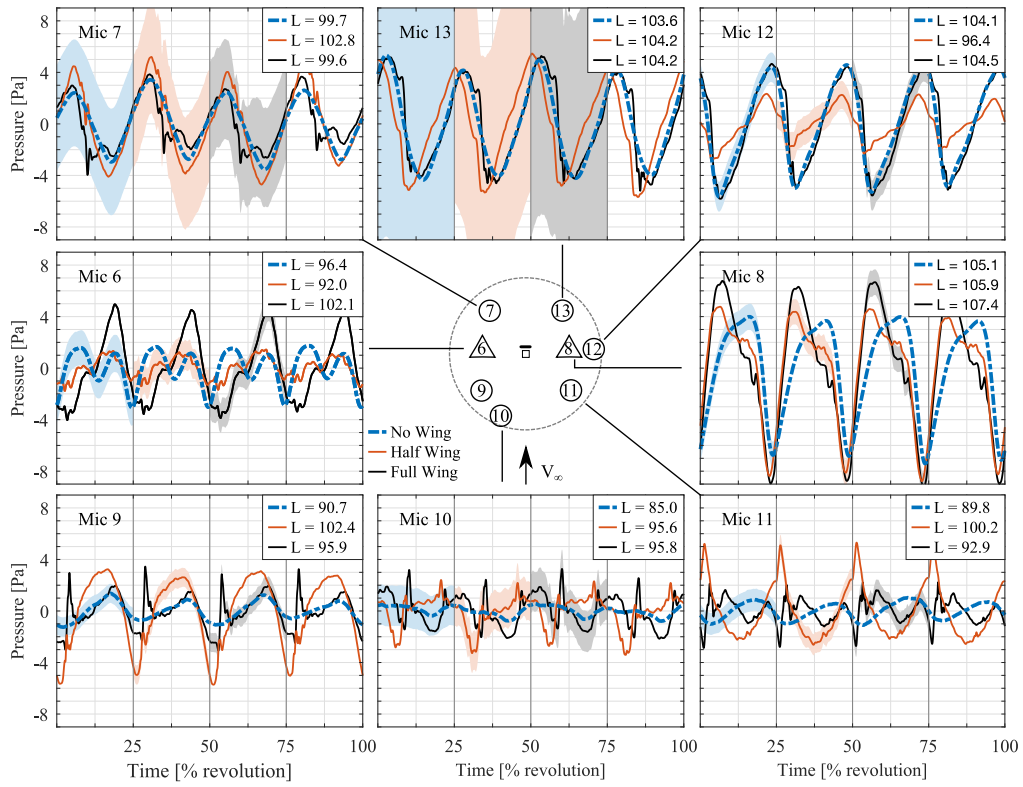
Figure 14. Wing configuration acoustic time history comparison for an operating condition of M_{TUN} = 0.111, Yaw = 0°, and Ω = 6500. No wing C_T = 0.183, C_P = 0.146; half wing C_T = 0.182, C_P = 0.145; full wing C_T = 0.184, C_P = 0.145. OASPL (L) provided on each subplot in units of dB.
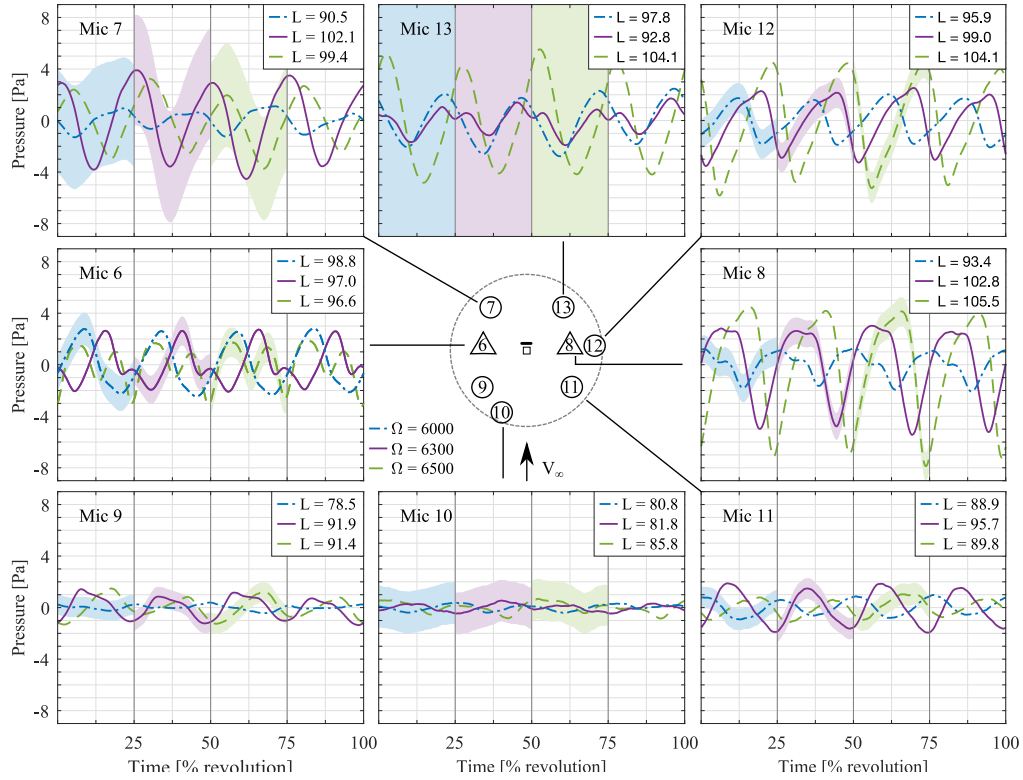
Figure 15. RPM sweep acoustic time history for the no wing configuration and a condition of M_{TUN} = 0.111, Yaw = 0°, and Ω = 6000-6500. Ω = 6000 condition had a C_T = 0.175 and C_P = 0.144, Ω = 6300 condition had a C_T = 0.181 and C_P = 0.146, and Ω = 6500 condition had a C_T = 0.184 and C_P = 0.147. OASPL (L) in units of dB.
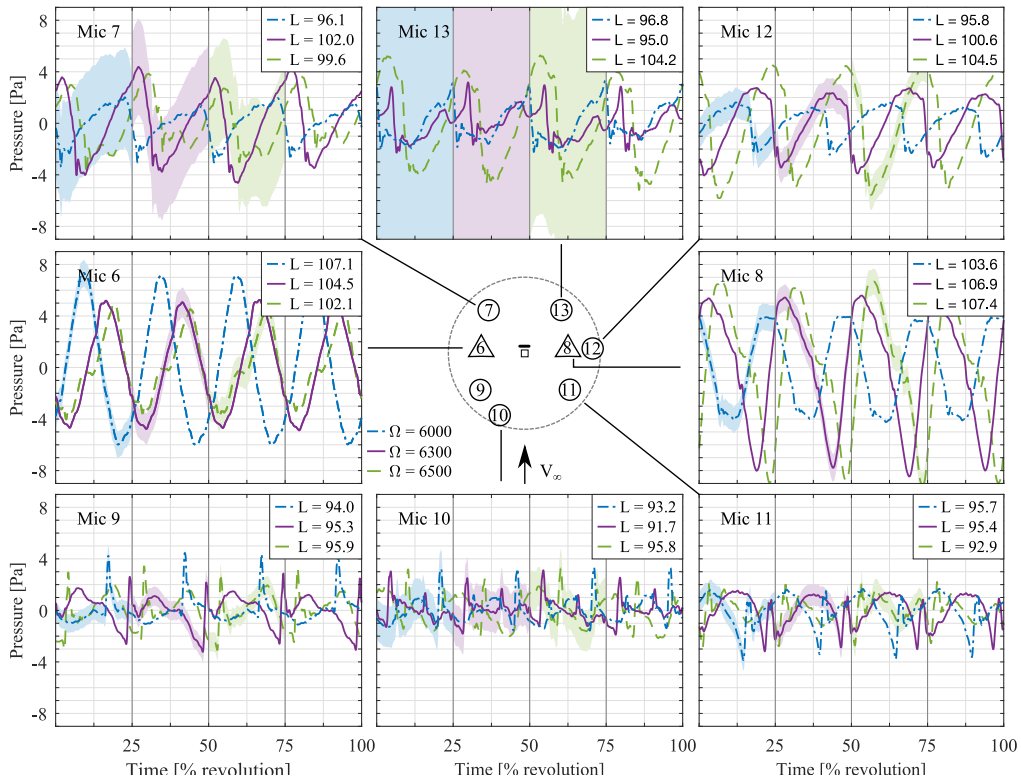
Figure 16. RPM sweep acoustic time history for the full wing configuration and operating condition of M_{TUN} = 0.111, Yaw = 0°, and Ω = 6000-6500. Ω = 6000 condition had a C_T = 0.175 and C_P = 0.143, Ω = 6300 condition had a C_T = 0.181 and C_P = 0.144, and Ω = 6500 condition had a C_T = 0.184 and C_P = 0.145. OASPL (L) provided on each subplot in units of dB (ref. 20 μPa).

A wind tunnel velocity sweep was also performed for the half wing and full wing configurations. Figure 18 shows the pressure time histories for all microphones for the full wing condition, and matching tunnel conditions from Fig. 17. Several important trends can be seen in Fig. 18. The first identifiable trend is that the in-plane microphone (6, 8, and 12) signals decrease with increasing tunnel Mach number. This is a complex situation, as the apparent direction of the microphones are changing from in-plane to slightly out of plane with increased tunnel speed. This means that thickness noise and loading noise are both at play, and for this condition, a reduction in the acoustic emissions is recorded.

The second major trend is the increasing acoustic emissions with increasing tunnel speed in the fore direction. The propeller steady loading decreases with increasing tunnel speed, as shown in the decreasing C_T values. However, the wing provides an increasingly impulsive loading on the propeller as the wing's wake deficit is proportional to tunnel speed. These competing factors have resulted in an initial decrease then increase in the noise for these sideline microphones in the forward direction, and a monotonically increasing amplitude in the forward direction (microphone 10). This is yet another area where computational modeling is required in order to help explain what combination of factors has significantly contributed to the complex and changing acoustic emissions.

Yaw Variation

A yaw variation of 0° and 5° was performed over various operating conditions and wing configurations. Figure 19 shows a sample yaw variation for the full wing configuration and an operating condition of M_{TUN} = 0.111, Yaw = 0° and 5°, and Ω = 6200. The resultant acoustic time history reveals either a slight increase or no change in the OASPL for the yaw of 5° compared to 0° for all microphones. The increase in noise is likely due to the yaw resulting in a generation of lift on the wing and subsequent increase in the size and deficit of the wing wake as well as the relative change in where the wake impinges on the propeller. In general, however, this small of a yaw angle produced no significant differences for this condition.

CONCLUSIONS

The Aerodynamic and Acoustic Rotorprop Test (AART) Program in the National Full-Scale Aerodynamics Complex (NFAC) 40-by 80-Foot Wind Tunnel was completed in July of 2020. Eight microphones and three beamform acoustic arrays were placed around a Sensenich L26H propeller and tested under various revolution rates, wind tunnel speeds, yaw conditions, and wing (no, half, and full) configurations. A pistol reflection test was conducted, and it was shown that all microphones had reflections likely caused by the tunnel floor,
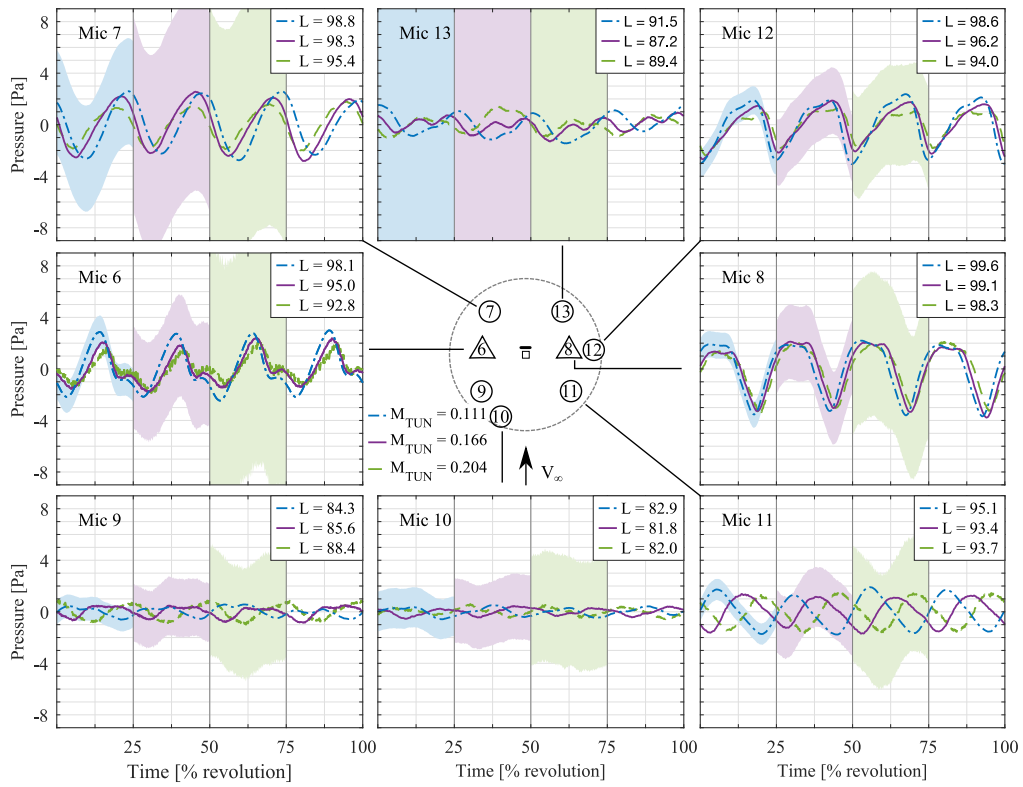
Figure 17. Acoustic time history for the no wing configuration and a wind tunnel speed sweep condition of M_{TUN} = 0.111-0.204, Yaw = 0°, and Ω = 6200. M_{TUN} = 0.111 condition had C_T = 0.178, C_P = 0.145; M_{TUN} = 0.166 condition had C_T = 0.112, C_P = 0.119; M_{TUN} = 0.204 condition had a C_T = 0.052, C_P = 0.077. OASPL (L) in units of dB.
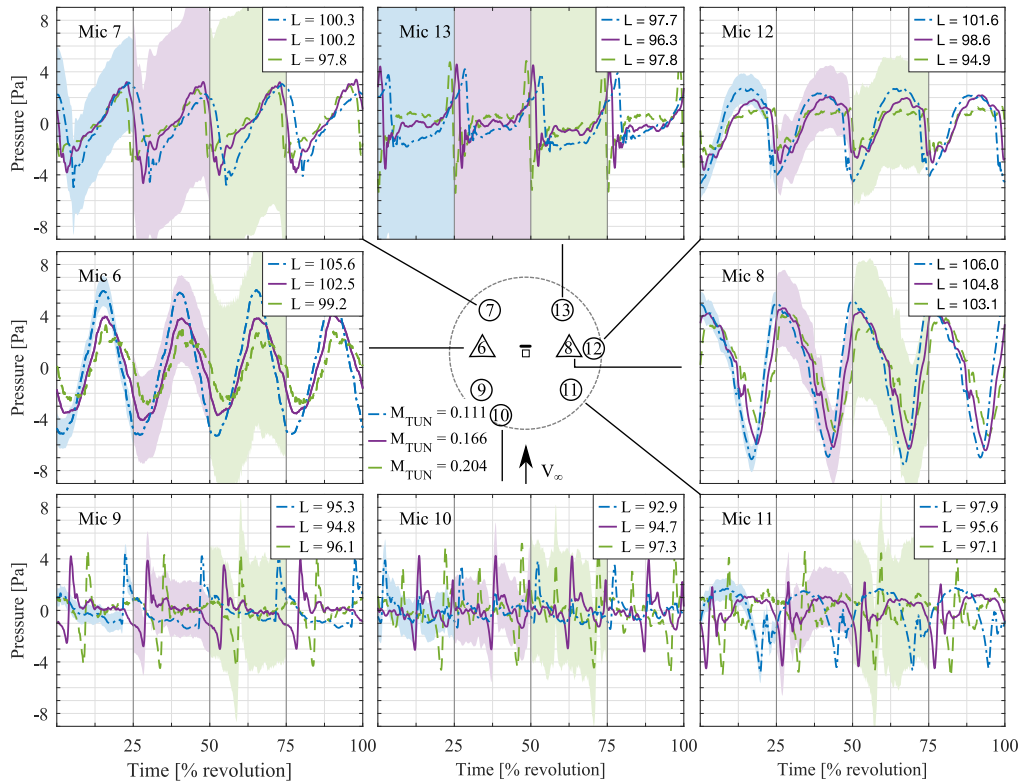
Figure 18. Acoustic time history for the full wing configuration and a wind tunnel speed sweep condition of M_{TUN} = 0.111-0.221, Yaw = 0°, and Ω = 6200. M_{TUN} = 0.111 condition had C_T = 0.179, C_P = 0.144; M_{TUN} = 0.166 condition had C_T = 0.117, C_P = 0.122; M_{TUN} = 0.204 condition had C_T = 0.058, C_P = 0.081. OASPL (L) in units of dB.
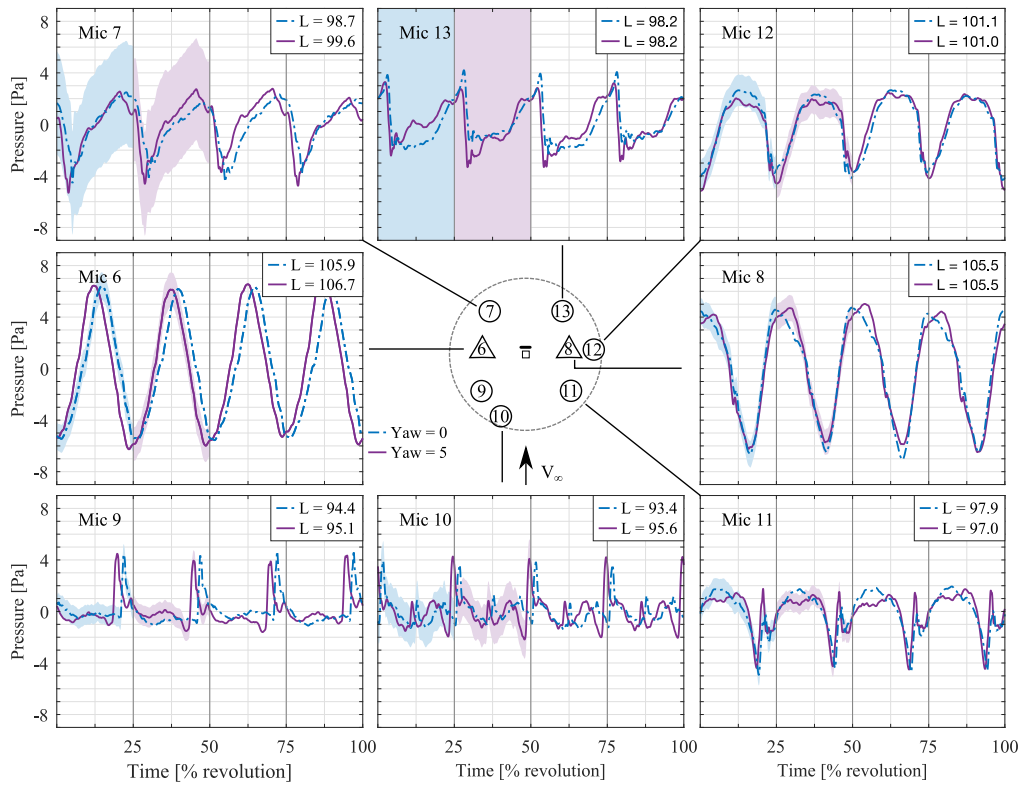
Figure 19. Yaw variation acoustic time history comparison for operating conditions of M_{TUN} = 0.111, Yaw = 0° and 5°, and Ω = 6200 for the full wing configuration. Yaw = 0° condition had a C_T = 0.179 and C_P = 0.144 and the Yaw = 5° condition had a C_T = 0.175 and C_P = 0.142. C_T and C_P for the yaw condition are not corrected for the angle relative to the free stream. OASPL (L) provided on each subplot in units of dB (ref. 20 μPa).

with reflections in Microphone 6 noted as being particularly prominent. A background noise measurement was conducted for all test conditions, where the background noise was measured with the correct tunnel and stand configuration, but with the L26H blades removed from the propeller hub. Quality signal-to-noise ratios were achieved for the wing configurations, especially at the lower tunnel Mach numbers.

Several significant concerns with the data have been noted throughout the paper. The first major concern is the effect that the reflections have on the recorded signals. The microphones were placed in close proximity (but still in the acoustic far-field) to the propeller due to signal-to-noise concerns, but that meant placing microphones on the facility turntable, which has less acoustic treatment than the rest of the facility. Further, the large metal plates that were used to secure the microphone stands to the tunnel floor may have contributed to these reflections, along with the wing and support structure.

The second major concern noted with this test was the strong influence of the flow and tunnel noise at the higher tunnel Mach numbers. Significant standard deviations were recorded at the higher tunnel Mach numbers due to revolution to revolution differences influenced by wind noise and other factors. However, at the lower Mach numbers, especially at M_{TUN} of 0.111, high quality data with low standard deviations were recorded.

The last major experimental concern is that data from micro-

phones 7 and 13 are almost universally lost due to ingesting the wake from upstream microphones. This is a lesson learned for the authors, as it is suspected that placing the microphones slightly further to either side would have negated this and resulted in higher quality measurements in similar directions.

With the significant data issues in mind, there are still positive takeaways from the AART acoustic experiment. It is clear from the data that the presence of an upstream body can significantly influence the acoustic emissions of a propeller system. Any unique change, as shown from the half wing to the full wing conditions, produces a unique acoustic emission from the propeller system. This is significant and shows that accurate modeling of the upstream bodies is required for correct acoustic emission predictions.

ACKNOWLEDGMENTS

REFERENCES

1. Booz-Allen and Hamilton, Inc., "Urban Air Mobility (UAM) Market Study," Contractor Report HQ-E-DAA-TN65181, NASA Langley Research Center, Hampton, VA, 2018.

2. Zawodny, N. S., Boyd, D. D., and Burley, C. L., "Acoustic Characterization and Prediction of Representative, Small-Scale Rotary-Wing Unmanned Aircraft System Components," Proceedings of the 72nd Annual Forum of the American Helicopter Society, West Palm Beach, FL, May 2016.

3. Stephenson, J. H., Watts, M. E., Greenwood, E., and Pascioni, K. A., "Development and Validation of Generic Maneuvering Flight Noise Abatement Guidance for Helicopters," Proceedings of the 76th Annual Forum of the Vertical Flight Society, Virginia Beach, VA, October 2020.

4. Zawodny, N. S., Boyd, D. D., and Nark, D. M., "Aerodynamic and Acoustic Interactions Associated with Inboard Propeller-Wing Configurations," AIAA Scitech 2021 Forum, 2021.

5. Herkes, W., "An Experimental Study of the Noise Generated by a Pusher Propeller Due to a Wake Entering the Propeller Disc," *von Karman Institute for Fluid Dynamics Rhode-Saint-Genese (Belgium)*, 1979.

6. Block, P., "Analysis of Noise Measured from a Propeller in a Wake," *NASA*, Vol. TP 2358, 1984.

7. Block, P., and Gentry Jr., G., "Directivity and Trends of Noise Generated by a Propeller in a Wake," *NASA*, Vol. TP 2609, 1986.

8. Soderman, P., and Horne, W., "Acoustic and Aerodynamic Study of a Pusher-Propeller Aircraft Model," *NASA*, Vol. TP 3040, 1990.

9. Marulo, F., Sollo, A., Aversano, M., Polimeno, U., and Perna, F., "Measurements and predictions of community noise of a pusher-propeller general aviation aircraft," Paper AIAA-2005-2984, 11th AIAA/CEAS Aeroacoustics Conference, Monterey, CA, May 2005.

10. Stephenson, J. H., Weitsman, D., and Zawodny, N. S., "Effects of flow recirculation on unmanned aircraft system (UAS) acoustic measurements in closed anechoic chambers," *The Journal of the Acoustical Society of America*, Vol. 145, (3), 2019, pp. 1153–1155.

11. Weitsman, D., Stephenson, J. H., and Zawodny, N. S., "Effects of flow recirculation on acoustic and dynamic measurements of rotary-wing systems operating in closed anechoic chambers," *The Journal of the Acoustical Society of America*, Vol. 148, (3), 2020, pp. 1325–1336.

12. Bowles, P., Matalanis, C., Wake, B., Berry, B., Bartz, E., and Scott, M., "A Model-Scale Wind-Tunnel Study of Main Rotor/Propeller Interference," Proceedings of the 72nd Annual Forum of the American Helicopter Society, West Palm Beach, FL, May 2016.

13. Barbely (Schatzman), N., Kitaplioglu, C., and Sim, B. W.-C., "Acoustics Reflections of Full-Scale Rotor Noise Measurements in NFAC 40- by 80-Foot Wind Tunnel," American Helicopter Society Specialists' Conference, San Francisco, CA, January 2012.

14. Burnside, N., and Horne, W., "Acoustic Surveys of a Scaled-Model CESTOL Transport Aircraft in Static and Forward Speed Conditions," Paper AIAA-2012-2231, 18th AIAA/CEAS Aeroacoustics Conference (33rd AIAA Aeroacoustics Conference), Colorado Springs, CO, June 2012.